**Earthquakes and Structures**, *Vol. 18, No. 3 (2020) 297-312*
DOI: https://doi.org/10.12989/eas.2020.18.3.297 

# Wave shape analysis of seismic records at borehole of TTRH02 and IWTH25 (KiK-net)

Shuichi Kamagata*

*Nuclear power department, Kajima Corporation, Tokyo 107-8348, Japan*

(*Received March 4, 2019, Revised September 5, 2019, Accepted February 4, 2020*)

**Abstract**. The KiK-net by NIED is a vertical array measurement system. In the database of KiK-net, singular pulse waves were observed in the seismic record at the borehole of TTRH02 during the mainshock (the magnitude of Japan Meteorological Agency ($M_J$) 7.3, $M_W$ 6.8) and aftershock ($M_j$ 4.2) of Tottori-ken Seibu earthquake in 2000. Singular pulse waves were also detected in the seismic records at the borehole of IWTH25 during the Iwate-Miyagi Nairiku earthquake in 2008 ($M_J$ 7.2, $M_W$ 6.9). These pulse waves are investigated by using the wave shape analysis methods, e.g., the non-stationary Fourier spectra and the double integrated displacement profiles. Two types of vibration modes are discriminated as the occurrence mechanism of the singular pulse waves. One corresponds to the reversal points in the displacement profile with the amplitude from $10^{-4}$ m to $10^{-1}$ m, which is mainly related to the fault activity and the amplification pass including the mechanical amplification (collision) of the seismograph in the casing pipe. The other is the cyclic pulse waves in the interval of reversal points, which is estimated as the backlash of the seismograph itself with the amplitude from $10^{-5}$ m to $10^{-4}$ m.

**Keywords:** wave shape analysis; non-stationary fourier spectra; band-pass filter; KiK-net; borehole; backlash of seismograph in casing pipe; pulse wave

## 1. Introduction

The K-NET and the KiK-net (strong-motion seismograph networks) were established in 1996 by the National Research Institute for Earth Science and Disaster Resilience (NIED 2018). More than 300 seismic events with $M_W$ greater than 6.0 were recorded since measurement began in 1996. The seismic records were referred by worldwide researchers (Papagiannopoulos, *et al*. (2013), Strasser *et al*. (2009)). The number of seismic events ($M_W$>6.0) and the maximum $M_W$ in each year are illustrated in Fig. 1. The KiK-net is the vertical array measurement system at the surface and the borehole. The present study focuses on the seismic records at the borehole as a database for the seismic design wave because the velocity of shear wave ($V_S$) at the borehole of most measurement sites satisfy the condition of engineering seismic bedrock ($V_S$ >700 m/s) for the nuclear power plants (NPPs) in Japan.

In the KiK-net database, peak acceleration values at the surface ($P_{A,\ S}$) greater than 20 m/s$^2$ were recorded in the seismic records of IWTH25 and AKTH04 during 2008 Iwate-Miyagi Nairiku earthquake. These values are considered as the background of the seismic design wave with the $P_A$ of 20 m/s$^2$ and more for the NPPs (NRA 2013a, b), which are apparently overestimated the seismic design wave. The author started the research of the occurrence mechanism of pulse waves with large $P_A$ in the seismic records.

Prior to my research the occurrence mechanism of the pulse waves with the $P_{A,\ S}$ of 38.7 m/s$^2$ at the surface in the up-down (U-D) component of IWTH25 has been investigated by many researchers. Aoi *et al*. (2010) explained it as the trampoline effect of the surface soil and Ohmachi *et al*. (2011) explained it as the rocking mode of the observation house. The author analyzed the pulse waves by the wave shape analysis and explained them as the induced vertical pulse waves by the uplift of observation house (Kamagata and Takewaki 2017).

The wave shape analysis was introduced from an engineering-based perspective and detected various occurrence mechanisms of the pulse waves with large $P_A$ in the seismic records as follows.

- The pulse wave with the $P_A$ of 6.8m/s$^2$ at the Kashiwazaki-Kariwa NPPs during the Niigata-ken Chuetsu-oki earthquake in 2007 was identified by the Ricker-wavelet (Ricker, 1942) and the collision between the building and the side soil was deduced. (JNES 2009, Kamagata, 2009, Kamagata and Takewaki 2013a, Kojima *et al*. 2014);
- Deterioration of the surface soil was deduced for $P_A$ of 4.38 m/s$^2$ at the Hamaoka NPPs during the Suruga-Bay earthquake in 2009 (Kamagata and Takewaki 2013b);
- The cyclic mobility phenomenon of liquefaction was deduced in the seismic records of Port Island during the Hyogo-ken Nanbu earthquake in 1995 (Kamagata and Takewaki 2015);
- The collision of the base-mat of the observation house and the side soil was deduced in the seismic record at

*Corresponding author, Ph.D.
E-mail: kamagata@kajima.com


 ISSN: 2092-7614 (Print), 2092-7622 (Online)

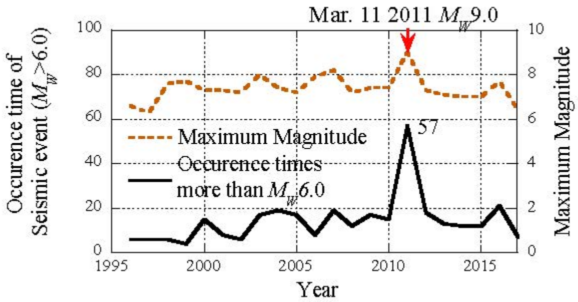


Fig. 1 Seismic events by K-NET KiK-net (NIED)

the surface of AKTH04 during 2008 Iwate-Miyagi Nairiku earthquake (Kamagata and Takewaki 2018).

In this study, the occurrence mechanism of singular pulse waves in the seismic records at the borehole of TTRH02 is investigated. The singular pulse waves are detected in the seismic records of the mainshock (moment magnitude: $M_W$ 6.8) and the aftershock (Japan Meteorological Agency magnitude; $M_J$ 4.2) during 2000 Tottori-ken Seibu earthquake but no singular pulse waves are detected in the seismic records during the seismic event ($M_W$ 6.6) on Oct. 21st, 2016. The frequency property of the singular pulse waves is investigated by using wave shape analysis. Further, the author evaluates the displacement amplitude ($P_{MD}$) of the singular pulse waves form the acceleration maximum amplitude ($P_{MA}$) and its frequency ($f_{MA}$) by the relation of $P_{MD}=P_{MA}/(2\pi f_{MA})^2$. The singular pulse waves with $10^{-4}$ m<$P_{MD,B}$<$10^{-1}$ m in $f_{MA,B}$<10Hz are estimated to be caused by the fault activity and the propagation pass including the mechanical amplification (collision) between the seismograph and the casing pipe. Further, the singular pulse waves with $10^{-5}$ m<$P_{MD,B}$<$10^{-4}$ m in 10Hz<$f_{MA,B}$ are estimated to be caused by the backlash of seismograph itself in the casing-pipe. In the seismic record at the borehole of IWTH25, singular pulse waves are detected in the filtered acceleration profile from 10Hz to 40Hz. The occurrence mechanism is deduced same with that of TTRH02 from the similarity of frequency, and the frequency caused by the backlash is estimated to be about 14Hz. These findings are applicable to select the database of the seismic records for the seismic design waves of the NPPs.

## 2. Non-stationary fourier spectra

The response envelope spectrum (Trifunac 1971) was proposed from the perspective of the structural engineering. In that study, the transient seismic response of the single degree of freedom (SDOF) model with various frequencies was illustrated in the contour figure with the horizontal axis of the duration time and the vertical axis of the frequency (period) of the model. In the wave shape analysis, the non-stationary Fourier (NSF) spectrum (Eq. (1)) was introduced as a type of moving-window spectrum, and maximum amplitude spectrum (Eq. (2)) was derived as a secondary spectrum of the NSF spectrum. The NSF spectrum is illustrated in the contour figure with the horizontal axis of the duration time and the vertical axis of the frequency. The contour level detects the amplitude normalized by the peak maximum amplitude.

$$F(\omega_i;t_j)=\int_{-\infty}^{\infty} g(\tau,t_j)\exp[-i\omega_i\,\tau]d\tau$$

where

$$g(\tau,t_j)=\ddot{y}(\tau);\quad t_j-t_a/2\le\tau\le t_j+t_a/2$$

$$g(\tau,t_j)=0;\quad \tau<t_j-t_a/2,\ t_j+t_a/2<\tau$$

$\ddot{y}(\tau)$; seismic record,

$t_j\ (j=1,2,\cdots M)$; $j$-th time, (1)

$\omega_i\ (i=1,2,\cdots N/2)$; $i$-th frequency,

$N$; number of steps in FFT analysis,

$M=T/\Delta T$; number of steps in sweep process,

$T$; duration time of seismic record (s),

$\Delta T$; sweep interval time (s),

$t_a$; data-window width (s).

$$S_{MA}(\omega_i)=\max\{F(\omega_i;\ t_j);t_j=t_1,\ldots,t_M\} \tag{2}$$

The analytical accuracy of the NSF spectrum was calibrated by the analytical results of one and two cycles of sinusoidal waves with the frequency of 1 Hz and the Ricker wavelet (Ricker (1942)) (Eq. (3); $f_C$=1Hz) as shown in Fig. 2(a).

$$f_R(t)=\left(1-f_C{}^2\,t^2/2\right)\exp\left(-f_C{}^2\,t^2/4\right) \tag{3}$$

Three pulse waves (see Fig. 2(a)) were analyzed by three cases of data-window width ($t_a$): 0.5s, 1.0s and 2.0s as shown in Fig. 2(b). In the maximum amplitude spectra of sinusoidal waves and the Ricker wavelet (see in Fig. 2(c)), the peak maximum amplitude ($P_{MA}$) and its frequency ($f_{MA}$) are listed as shown in Table 1.

The data-window width ($t_a$) affects the analytical results of maximum amplitude as follows.

- The $P_{MA}$ of one cycle of sinusoidal wave were 1.04m/s$^2$ by $t_a$=1.0s and 2.0s, which is correctly evaluated the amplitude of sinusoidal wave.
- The $P_{MA}$ of two cycles of sinusoidal wave by $t_a$=1.0s was 1.04m/s$^2$, which is correctly evaluated the amplitude of sinusoidal wave. On the other hand, the $P_{MA}$ by $t_a$=2.0s was 2.0m/s$^2$, which is two times overestimated.
- In the maximum amplitude spectra of the Ricker wavelet, the $P_{MA}$; the $f_{MA}$ were 0.74m/s$^2$; 1.17Hz by $t_a$=1.0s and 0.83m/s$^2$; 1.03Hz by $t_a$=2.0s. The $t_a$=2s was longer than the duration time of Ricker wavelet and can correctly evaluate the amplitude but cannot correctly evaluated the occurrence time of peak value.

Above analytical results suggest that the $t_a$ should be close to the period ($1/f_{MA}$) of the dominant component, therefore the selection condition of the suitable $t_a$ was defined as minimum $t_a>1/f_{MA}$. The suitable $t_a$ were selected in three waves and the NSF spectra with the suitable $t_a$ are enclosed by dotted rectangle in Fig. 2.

In the seismic records the dominant components were

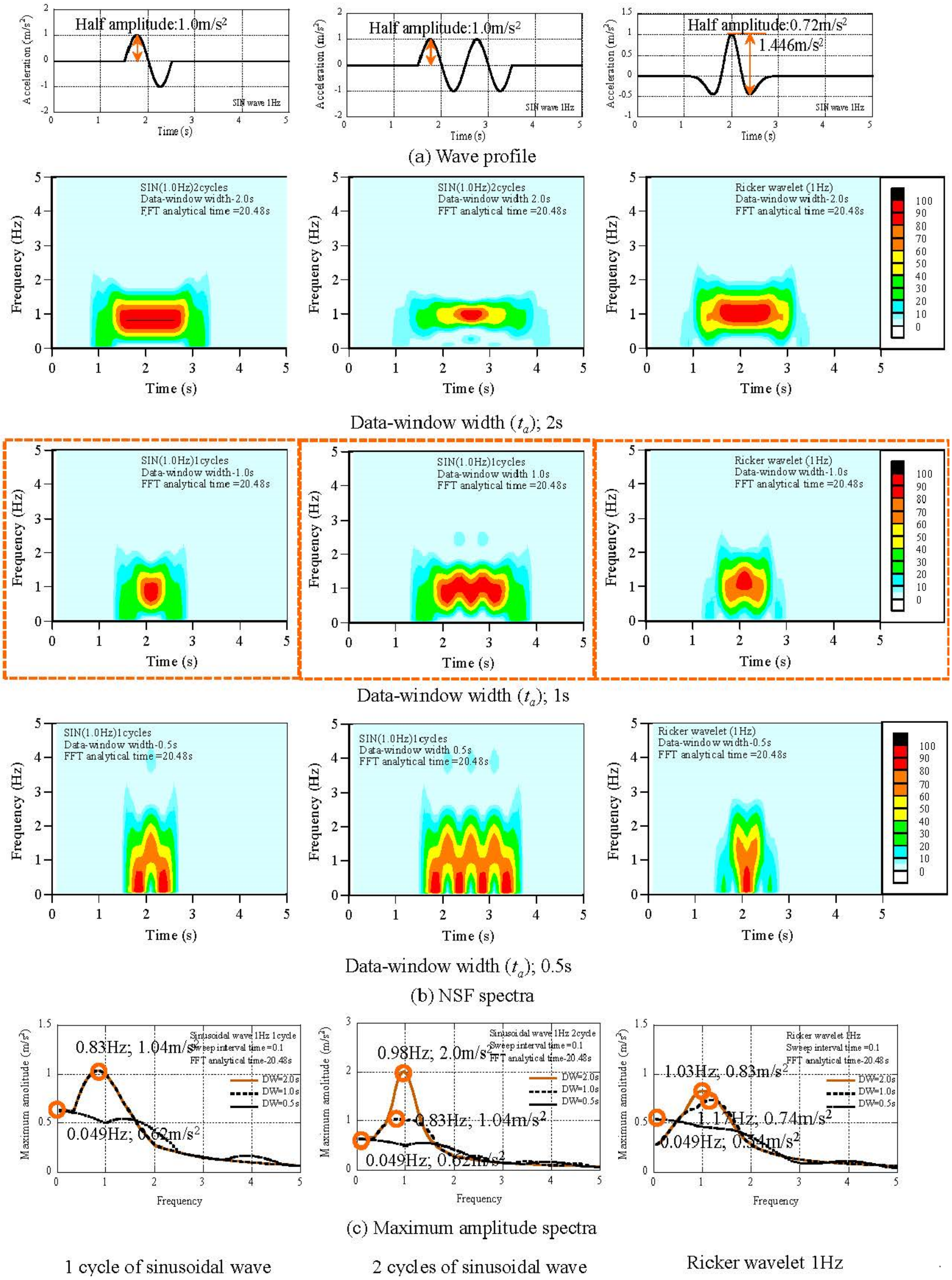


Fig. 2 Calibration of data-window width ($t_a$) in NSF spectra

scattered in the frequency range, therefore, the author introduced a new analytical process in order to improve the analytical accuracy of the NSF spectra as follows.

- Pre-processing of seismic record to the filtered acceleration profile by the band-pass filter.
- Parametric analysis by the data-window width ($t_a$)
- Selection of the suitable $t_a$ by the condition of minimum $t_a > 1/f_{MA}$.

## 3. Singular pulse waves in seismic records at borehole of KiK-net

This study focuses on the seismic records at the borehole of KiK-net because the velocity of the shear wave ($V_S$) at the boreholes of most measurement sites satisfies the condition of the engineering seismic bedrock ($V_S$>700 m/s²) for the NPPs in Japan. In revised regulatory requirements

Table 1 Peak maximum amplitude ($P_{MA}$ (m/s$^2$)) and frequency ($f_{MA}$ (Hz))

| $t_a$ (s) | $1/t_a$ (Hz) | One cycle SIN wave | | Two cycles SIN wave | | Ricker wavelet | |
|---|---|---|---|---|---|---|---|
| | | $P_{MA}$ | $f_{MA}$ | $P_{MA}$ | $f_{MA}$ | $P_{MA}$ | $f_{MA}$ |
| 0.5 | 2.0 | 0.62 | 0.049 | 0.62 | 0..049 | 0.54 | 0.049 |
| 1.0 | 1.0 | 1.04 | 0.83 | 1.04 | 0.83 | 0.74 | 1.17 |
| 2.0 | 0.5 | 1.04 | 0.83 | 2.0 | 0.98 | 0.83 | 1.03 |

Table 2 Seismic records with $P_{A,S}$ greater than 10 m/s$^2$ by unspecified active faults

| Name of earthquake | $M_W$ | Depth(km) | Site code | Epicentral distance (km) | Synthesis $P_{A,S}$ (m/s$^2$) |
|---|---|---|---|---|---|
| 2008 Iwate-Miyagi Nairiku | 6.9 | 8 | IWTH25 | 3 | 40.22 |
| | | | AKTH04 | 22 | 26.00 |
| | | | IWTH26 | 12 | 10.29 |
| 2000 Tottori-ken Seibu | 6.8 | 11 | TTRH02 | 12 | 11.42 |
| 2011 Ibaragi-ken Hokubu | 5.8 | 5 | IBRH13 | 1 | 10.84 |
| 2013 Tochigi-ken Hokubu | 5.8 | 3 | TCGH07 | 4 | 13.00 |
| 2011 Wakayama-ken Hokubu | 5.0 | 7 | WKYH01 | 2 | 10.84 |

Table 3 Peak acceleration ($P_A$ (m/s$^2$)) at surface and borehole of TTRH02 and IWTH25

| Site | N-S | | E-W | | U-D | | Seismic event | $M_W$ | Epicentral Distance (km) |
|---|---|---|---|---|---|---|---|---|---|
| | $P_{A,S}$ | $P_{A,B}$ | $P_{A,S}$ | $P_{A,B}$ | $P_{A,S}$ | $P_{A,B}$ | | | |
| TTRH02 | 9.24 | 3.57 | 7.56 | 5.74 | 7.76 | 3.18 | 2000 Tottori-ken Seibu | 6.8 | 12 |
| IWTH25 | 11.43 | 10.36 | 14.33 | 7.48 | 38.7 | 6.81 | 2008 Iwate-Miyagi Nairiku | 6.9 | 3 |

Table 4 Band-pass filter and data-window width ($t_a$)

| Case | $f_{L1}$ (Hz) | $f_{L2}$ (Hz) | $f_{L3}$ (Hz) | $f_{L4}$ (Hz) | $t_a$ (s) Case a | Case b | Case c |
|---|---|---|---|---|---|---|---|
| 1 | 0.2 | 0.5 | 2.0 | 3.0 | 1.0 | 1.5 | 2.0 |
| 2 | 1.5 | 2.0 | 5.0 | 6.0 | 0.3 | 0.4 | 0.5 |
| 3 | 4.0 | 5.0 | 10.0 | 11.0 | 0.12 | 0.16 | 0.2 |
| 4 | 9.0 | 10.0 | 40.0 | 50.0 | 0.06 | 0.08 | 0.1 |

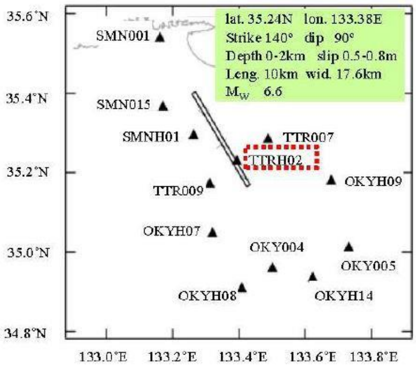


(a) Fault plane of 2000 Tottori-ken Seibu earthquake by PARI (2022) and Horikawa *et al*. (2001)

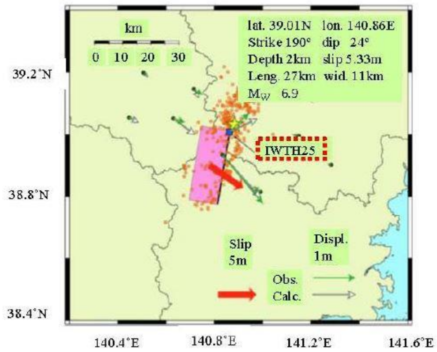


(b) Fault plane of 2008 Iwate-Miyagi Nairiku earthquake by NIED (2008)

Fig. 3 Seismic events of TTRH02 and IWTH25

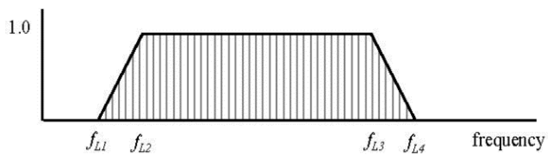


Fig. 4 Seismic events by K-NET KiK-net (NIED)

for light water NPPs in Japan the soundness of NPPs is certified for two types of seismic events, i.e., with and without a specified hypocenter (NRA 2013(b)). Seismic events occurring at unspecific active faults were selected by Japan Nuclear Energy Safety Organization (Kobayashi *et al*. 2014). Of these seismic events, seven seismic records with peak acceleration ($P_A$) greater than 10 m/s$^2$ were selected from database of the KiK-net, as shown in Table 2.

The influence of pulse-like waves was investigated in seismic design (Chang Hai *et al*. (2016), Rahgozar N. and Aziminejad A. (2016), Tajammolian H. Khoshnoudian and Bokaeian (2016)). In the selected data, peak acceleration values at the borehole ($P_{A,B}$) greater than 5 m/s$^2$ were detected in TTRH02 (E-W) and in IWTH25 (N-S; E-W and U-D), as shown in Table 3. The large $P_A$ at the borehole of IWTH25 are likely to be related to the short epicentral distance of 3km. Both measurement sites are illustrated with the fault plane (GSI 2008, AIST 2018) in Figs. 3(a) and 3(b). In order to identify the properties of the pulse waves, the seismic records were decomposed to filtered filtered acceleration profiles of Case 1, 2, 3 and 4 by using the band-pass filter as shown in Fig. 4 and Table 4. The $t_a$ of Case c was set to $1/f_{L2}$.

### *3.1 Seismic records of TTRH02*

The filtered acceleration profiles at the surface and the borehole of TTRH02 by the band-pass filter with $f_{L1}$ =0.5 Hz, $f_{L2}$ =1 Hz, $f_{L3}$ =40 Hz and $f_{L4}$ =50 Hz are illustrated as Case 0 with the Case-1, 2, 3 and 4 as shown in Fig. 5(a).

Generally, the seismic waves are amplified in the

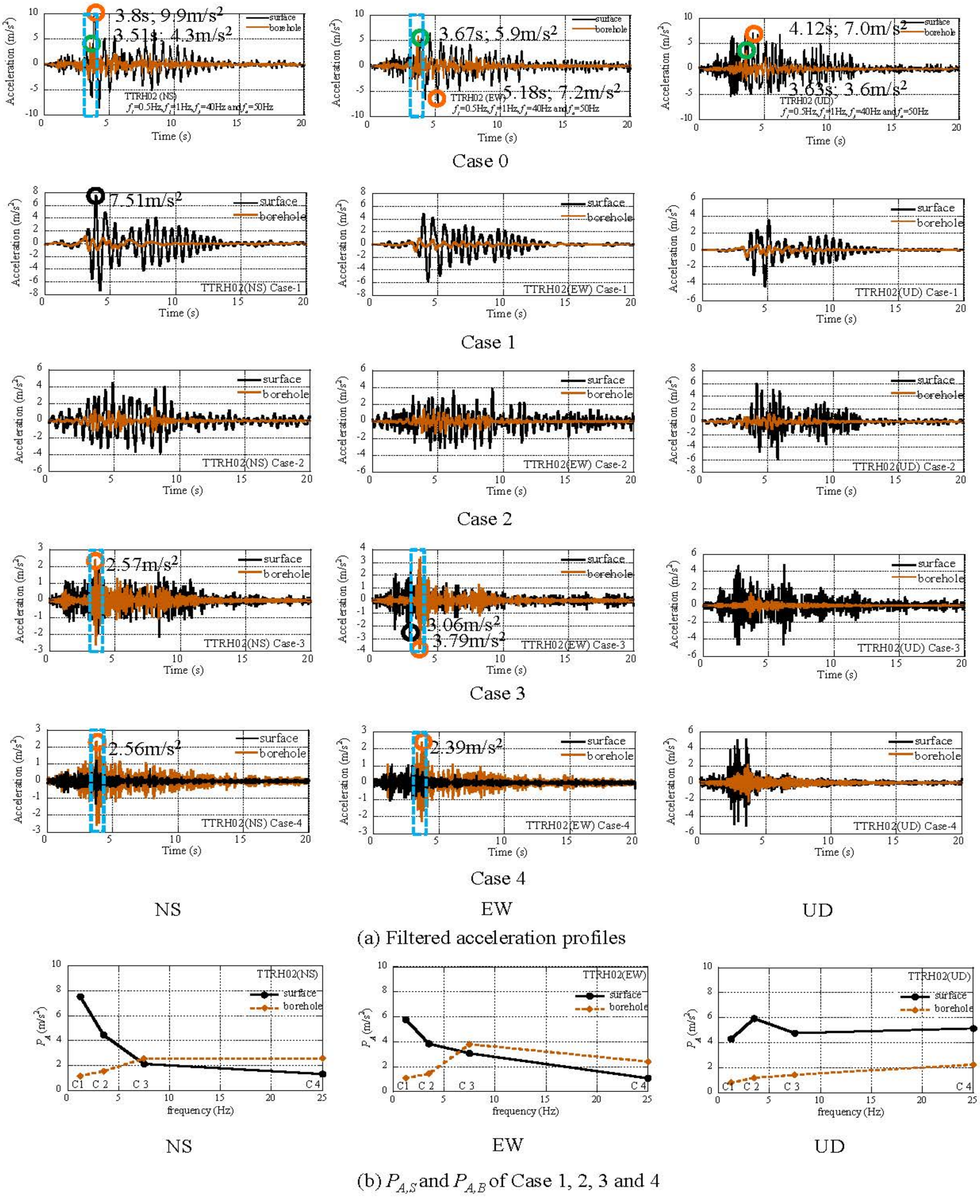


Fig. 5 Filtered acceleration profiles and PA at surface and borehole of TTRH02

propagation process from the borehole to the surface. The singular pulse waves at the borehole were detected in Case 3 and 4 (surround with a blue dotted frame), in which the pulse waves at the borehole exceeded those at the surface.

This study focused on the local amplification at the borehole of horizontal component namely $P_{A,B}$(N-S) of 4.3 m/s$^2$ at 3.51s and $P_{A,B}$(E-W) of 5.9m/s$^2$ at 3.67s. The $P_{A,S}$ and the $P_{A,B}$ of Case 1, 2, 3 and 4 are illustrated

Table 5 Peak acceleration values ($P_A$; m/s$^2$), $R_P$ and $R_{S/B}$ in acceleration profiles of TTRH02

| *case* | N-S | | | E-W | | | U-D | | |
|---|---|---|---|---|---|---|---|---|---|
| | $P_{A,S}$; $R_P$ | $P_{A,S}$; $R_P$ | $R_{S/B}$ | $P_{A,S}$; $R_P$ | $P_{A,S}$; $R_P$ | $R_{S/B}$ | $P_{A,S}$; $R_P$ | $P_{A,S}$; $R_P$ | $R_{S/B}$ |
| 0 | 9.9; 1.00 | 4.3; 1.00 | 2.3 | 7.2; 1.00 | 5.9; 1.00 | 1.22 | 7.0; 1.00 | 3.6; 1.00 | 1.94 |
| 1 | 7.5; **0.76** | 1.2; 0.28 | **6.4** | 5.8; **0.81** | 1.1; 0.19 | **5.4** | 4.3; **0.61** | 0.8; 0.22 | **5.4** |
| 2 | 4.5; 0.45 | 1.5; 0.35 | 2.9 | 3.9; **0.54** | 1.5; 0.25 | 2.7 | 5.9; **0.85** | 1.2; 0.33 | **5.1** |
| 3 | 2.2; 0.22 | 2.6; **0.60** | **0.84** | 3.1; 0.43 | 3.8; **0.64** | **0.81** | 4.8; **0.68** | 1.4; 0.39 | 3.4 |
| 4 | 1.3; 0.13 | 2.6; **0.60** | **0.51** | 1.1; 0.15 | 2.4; 0.41 | **0.45** | 5.1; **0.73** | 2.2; **0.62** | 2.3 |

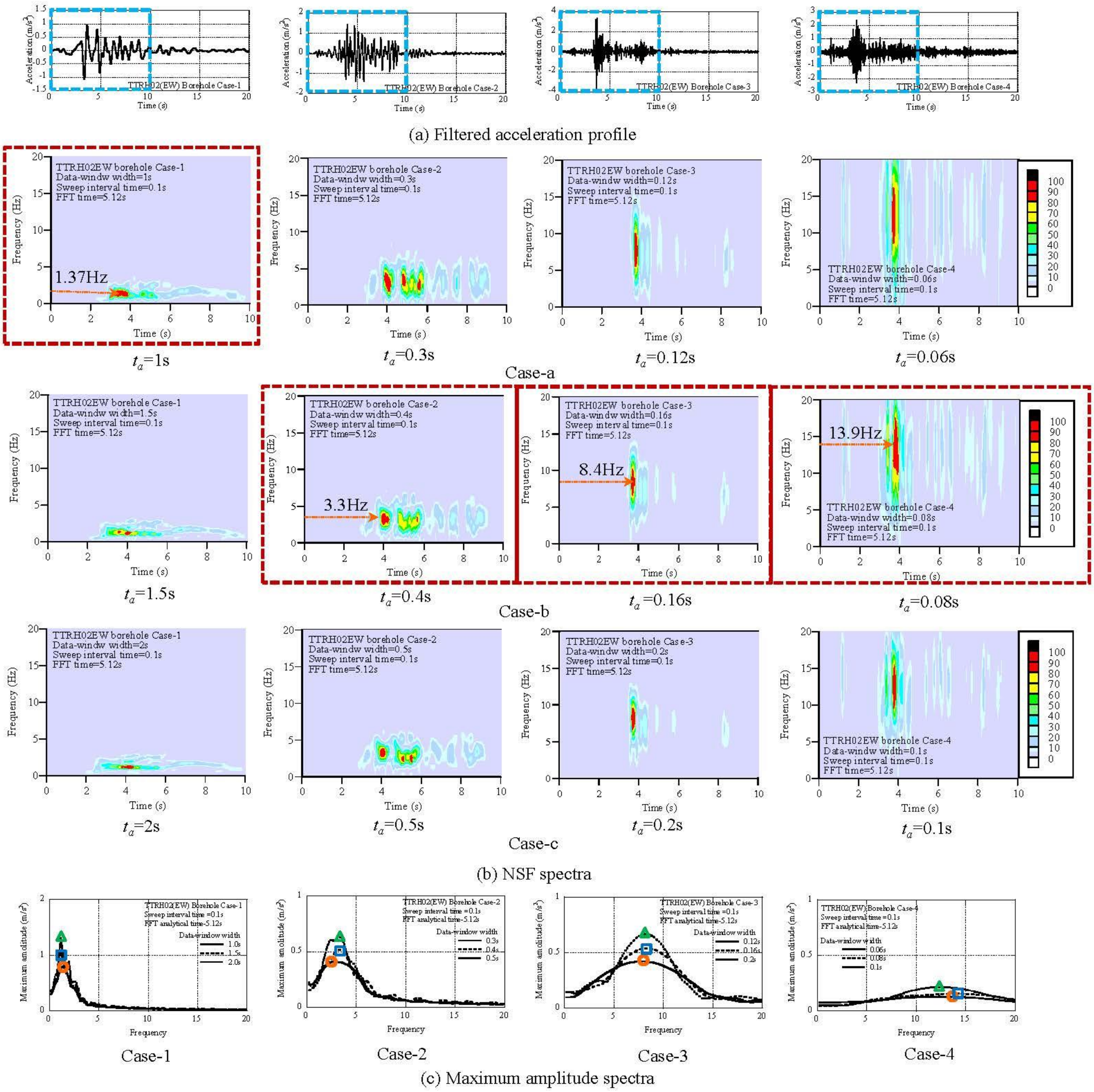


Fig. 6 Parametric analysis by $t_a$; TTRH02(E-W)

coupling with the frequency of $(f_{L2}+f_{L3})/2$, as shown in Fig. 5(b). The $P_{A,S}$, the $P_{A,B}$, and the $R_{S/B}$ ($P_{A,S}/P_{A,B}$) of Case 1, 2, 3, 4 are listed in Table 5. Further, the $P_A$ of Case 1, 2, 3 and 4 are compared with the $P_A$ of Case 0 as the $P_A$ ratio ($R_P$) of four frequency ranges.

The singular pulse waves were extracted by the condition of the P.R. greater than 50% and the $R_{S/B}$ smaller than 1.0 and larger than 5.0 (bold letters in Table 5).

Table 6 Selection of suitable $t_a$

| Case | Case 1 | | | Case 2 | | | Case 3 | | | Case 4 | | |
|---|---|---|---|---|---|---|---|---|---|---|---|---|
| | $f_{MA}$ | | $1/t_a$ | $f_{MA}$ | | $1/t_a$ | $f_{MA}$ | | $1/t_a$ | $f_{MA}$ | | $1/t_a$ |
| a | **1.37** | > | **1.0** | 2.7 | < | 3.3 | 7.8 | < | 8.3 | 12.3 | < | 16.7 |
| b | 1.17 | > | 0.67 | **3.3** | > | **2.5** | **8.4** | > | **6.25** | **13.9** | > | **12.5** |
| c | 1.17 | > | 0.5 | 3.3 | > | 2.0 | 8.2 | > | 5.0 | 12.5 | > | 10.0 |

Table 7 $P_{MA,\,S}$(m/s$^2$), $P_{MA,\,B}$ (m/s$^2$) and $R_{S/B}$ in NS, EW and UD components; TTRH02

| *case* | N-S | | | E-W | | | U-D | | |
|---|---|---|---|---|---|---|---|---|---|
| | $P_{MA,\,S}$ | $P_{MA,\,B}$ | $R_{S/B}$ | $P_{MA,\,S}$ | $P_{MA,\,B}$ | $R_{S/B}$ | $P_{MA,\,S}$ | $P_{MA,\,B}$ | $R_{S/B}$ |
| 1 | 6.9 | 1.03 | 6.70 | 5.2 | 0.80 | 6.50 | 4.0 | 0.69 | 5.80 |
| 2 | 1.24 | 0.44 | 2.82 | 1.60 | 0.52 | 3.08 | 2.1 | 0.47 | 4.47 |
| 3 | 0.37 | 0.40 | **0.93** | 0.50 | 0.54 | **0.93** | 0.94 | 0.25 | 3.76 |
| 4 | 0.11 | 0.22 | **0.50** | 0.076 | 0.16 | **0.48** | 0.36 | 0.13 | 2.77 |

• In N-S component the $R_{S/B}$ in Case 1 was 6.4 ($P_{A,\,S}$> $P_{A,\,B}$), which was considered as a natural amplification

• in the surface soil. The $R_{S/B}$ in Cases 3 and 4 are 0.84 and 0.51 ($P_{A,\,S}$ < $P_{A,\,B}$), which suggested an unnatural amplification at the borehole.

• In E-W component, the $R_{S/B}$ in Cases 1 and 2 were 5.4 and 2.7 ($P_{A,\,S}$ > $P_{A,\,B}$), which were also considered as a natural amplification in the surface soil as well as the N-S component. The $R_{S/B}$ in Case 3 and Case 4 were 0.81 and 0.45 ($P_{A,\,S}$ < $P_{A,\,B}$), which suggested an unnatural amplification as well as N-S component.

• In U-D component, the $P_{A,\,S}$ in Case 1, 2, 3 and 4 were greater than 4.0 m/s$^2$, which were considered as the mechanical amplification namely the rocking mode of the observation house (Ohmachi *el al*. 2011) and the induced vertical pulse waves by the up-lift of the observation house (Kamagata and Takewaki 2017). The $P_{A,\,B}$ of 2.2 m/s$^2$ in Case 4 was the largest in four cases but the $R_{S/B}$ of 2.3 ($P_{A,\,S}$ >$P_{A,\,B}$) was minimum in four cases, which were resulted in the mechanical amplification by the observation house at the surface.

• In Fig. 5(b) the $P_{A,\,B}$ in Case 3 and 4 were larger than the $P_{A,\,S}$ in N-S and E-W components and the $P_{A,\,S}$ in every case were larger than the $P_{A,\,B}$ in U-D component.

Newly introduced analytical process of selection of suitable $t_a$ in the NSF spectra were certified by the analytical results at the borehole of TTRH02 (E-W). The filtered acceleration profiles at the borehole of TTRH02 (E-W) are illustrated in Fig. 6(a) and the pulse waves (enclosed by dotted blue rectangle) was analyzed by the NSF spectra. The data-window width ($t_a$) of Case a, b and c were set for Case 1, 2, 3 and 4 as shown in Table 4. Each NSF spectrum of Case 1, 2, 3 and 4 with three cases of $t_a$ was calculated by 100 steps of FFT analysis in the duration time of 10s, and thus total 1200 times of FFT analysis were calculated and they are illustrated as shown in Fig. 6(b). The maximum amplitude spectra of Case a, b and c are compared as shown in Fig. 6(c). The $f_{MA}$ of Case a, b and c were compared with frequency of $1/t_a$ as shown in Table 6, in which the suitable $t_a$ (bold letters) were selected by the condition of minimum $t_a$ >$1/f_{MA}$. The selected NSF spectra are enclosed by dotted red rectangle. Similar analytical process was conducted for the seismic records at the surface.

The acceleration profiles at the surface and the borehole of Case 1, 2, 3 and 4 are illustrated in Fig. 7(a). The pulse waves (enclosed by dotted blue rectangle) were analyzed by the NSF spectra with three cases of $t_a$. The NSF spectra of the suitable $t_a$ at the surface and the borehole are illustrated in Fig.7(b) and (c). The maximum amplitude spectra at the surface and the borehole are compared in Fig. 7(d). The $P_{MA,\,S}$, the $P_{MA,\,B}$ and the $R_{S/B}$ of Case 1, 2, 3 and 4 in N-S, E-W and U-D components are listed in Table 7. The singular $R_{S/B}$ (bold letters) were detected in Case 3 and 4 by the condition of the $R_{S/B}$< 1.0, which was considered as an unnatural amplification at the borehole.

The properties of the dominant components were evaluated as follows.

• In Cases 1 and 2, the $P_{MA,\,S}$ were greater than the $P_{MA,\,B}$, and the occurrence time of the $P_{MA,\,S}$ were later than those of the $P_{MA,\,B}$, which was considered as the natural amplification in the propagation process from the borehole to the surface.

• In Cases 3 and 4, the $P_{MA,\,S}$ occurred earlier than the $P_{MA,\,B}$ and the $P_{MA,\,B}$ were larger than the $P_{MA,\,S}$, which suggested an unnatural amplification at the borehole.

• The singular pulse waves at the borehole was confirmed in the maximum amplitude spectra of Case 3 and 4, which was estimated as an unnatural amplification at the borehole in the frequency range of 5Hz or more.

### *3.2 Seismic records of TTRH02 in after-shock in 2000 and seismic event in 2016*

The author investigated the seismic records of TTRH02 in the database of KiK-net and focused on the following three seismic records:

• at the seismic event ($M_W$ 6.8) on October 6, 2000 (main-shock),

• at the seismic event ($M_J$ 4.2) on October 17, 2000 (after-shock), and

• at the seismic event ($M_W$ 6.6) on October 21, 2016.

In this section, the double integrated displacement profile, which is one of the analysis methods in the wave shape analysis, was adopted to make clear the vibration state of the pulse waves. The filtered acceleration profiles of case-0 (brown line) are illustrated with the double integrated displacement profiles (black line) as shown in Fig. 8(a). Further, the filtered acceleration profiles of Case 4 at the surface (brown line) and the borehole (black line) are compared in Fig. 8(b). The $P_{A,\,S}$, the $P_{A,\,B}$ and the $R_{S/B}$ ($P_{A,\,S}/P_{A,\,B}$) of case 4 are listed in Table 8.

The properties of pulse waves in three seismic events were evaluated as follows.

• In the main-shock, the positive and negative pulse waves of the $P_{A,\,B}$>2 m/s$^2$, (marked by arrows; positive; red and negative; green in Fig.8 (a)) corresponded to the reversal points (marked by circle) in the displacement profile.

• In the after-shock, the cyclic pulse waves with the $P_{A,\,B}$>0.2 m/s$^2$ occurred in the interval between the reversal points of the $P_{D,\,B}$>0.0003 m.

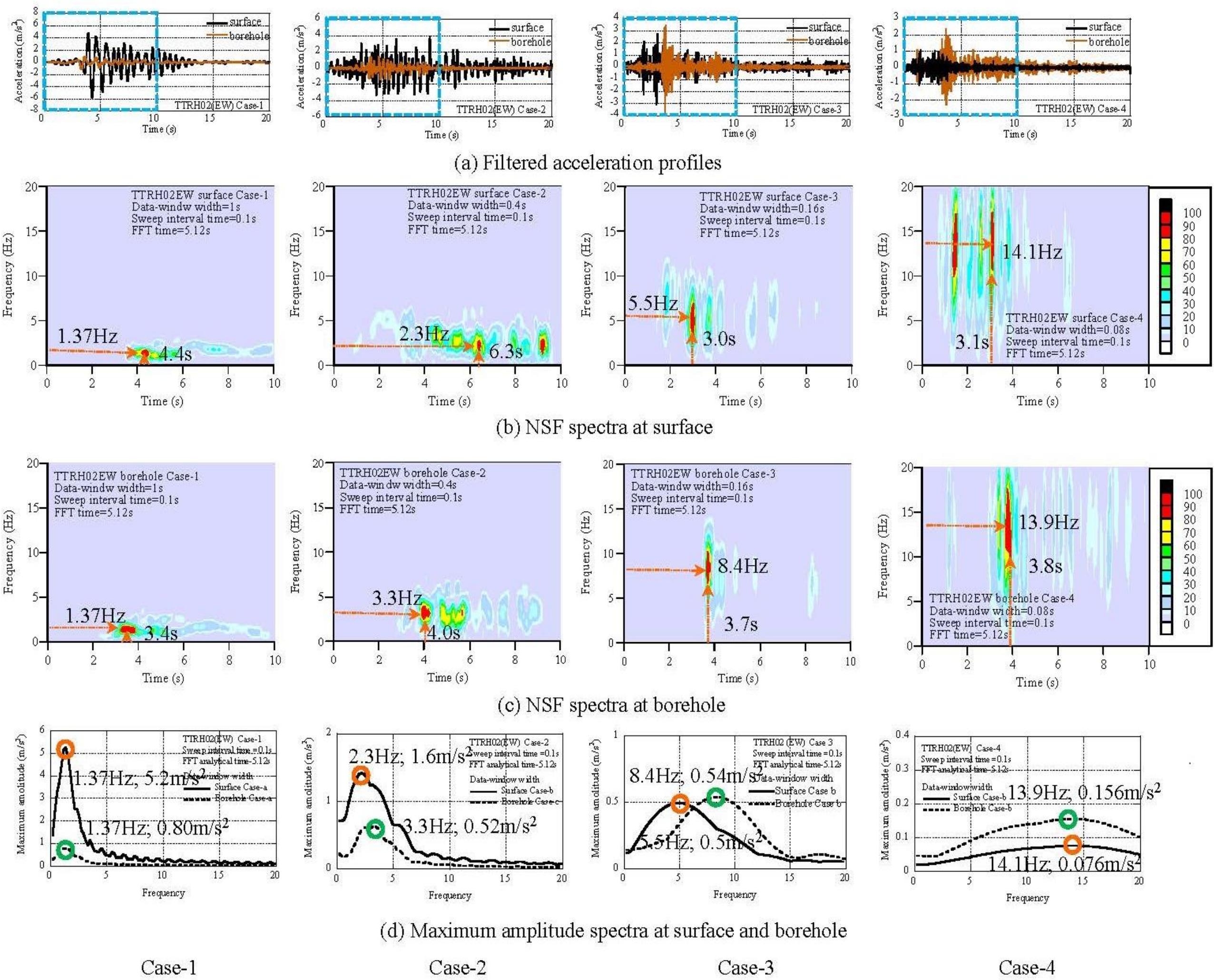


Fig. 7 NSF spectra of filtered acceleration profiles; TTRH02 (EW)

• In the seismic record (2016), the pulse waves with the $P_{A,B} > 0.1\text{m/s}^2$ corresponded to the reversal points in the displacement profiles as well as the main-shock, but no singular pulse waves were detected at the borehole although the $P_{D,B}$ of 0.001m and more was larger than the $P_{D,B}$ in the after-shock.• In the filtered acceleration profile of Case 4, the $P_{A,B}$ was larger than the $P_{A,S}$ in the main-shock and the after-shock, but the $P_{A,B}$ was smaller than the $P_{A,S}$ in the seismic event (2016).

• The $R_{S/B}$ was less than 1.0 ($P_{A,S} < P_{A,B}$) in the main-shock and the after-shock, which suggested an unnatural amplification at the borehole.

The $R_{S/B}$ was less than 1.0 ($P_{A,S}<P_{A,B}$) in the main-shock and the after-shock, which suggested an unnatural amplification at the borehole.

Further, the filtered acceleration profiles of Case 4 at the surface and the borehole (enclosed by dotted blue rectangle in Fig. 8(b)) were analyzed by the NSF spectra, as shown in Fig. 8(c). The maximum amplitude spectra of three seismic events are compared in Fig. 8(d). And the $f_{MA}$, the $P_{MA}$ at the surface and the borehole and the $R_{S/B}$ are listed in Table 9.

The properties of the dominant components were evaluated from the maximum amplitude spectra as follows.

Table 8 $P_{A,S}$, $P_{A,B}$ and $R_{S/B}$ of TTRH02 (case 4)

| Main-shock; E-W | | | After-shock; N-S | | | 2016; N-S | | |
|---|---|---|---|---|---|---|---|---|
| $P_{A,S}$ | $P_{A,B}$ | $R_{S/B}$ | $P_{A,S}$ | $P_{A,B}$ | $R_{S/B}$ | $P_{A,S}$ | $P_{A,B}$ | $R_{S/B}$ |
| 1.07 | 2.39 | **0.45** | 0.27 | 0.41 | **0.66** | 0.41 | 0.071 | 5.8 |

Table 9 $f_{MA}$ (Hz), $P_{MA}$ (m/s$^2$) and $R_{S/B}$ of TTRH02;Case 4

| | $f_{MA,S}$ | $P_{MA,S}$ | $f_{MA,B}$ | $P_{MA,B}$ | $R_{S/B}$ |
|---|---|---|---|---|---|
| Main-shock 2000 | 12.1 | $7.8\times10^{-2}$ | 12.9 | $2.4\times10^{-1}$ | **0.33** |
| After-shock 2000 | 12.9 | $2.7\times10^{-2}$ | 16.8 | $4.8\times10^{-2}$ | **0.68** |
| Seismic event 2016 | 12.5 | $3.4\times10^{-2}$ | 13.1 | $6.4\times10^{-3}$ | **5.3** |

• The $f_{MA,S}$ of three seismic events were scattered in a narrow frequency range from 12.1Hz to 12.9Hz, which were considered as the natural frequency of the surface soil.

• The $f_{MA,B}$ were scattered in higher frequency range from 12.9Hz 10 16.8Hz than the $f_{MA,S}$, in which the $f_{MA,B}$ of16.8Hz in the after-shock was singular in three seismic events.

• The $P_{MA,S}$ were scattered in the order of $10^{-2}\text{m/s}^2$, on

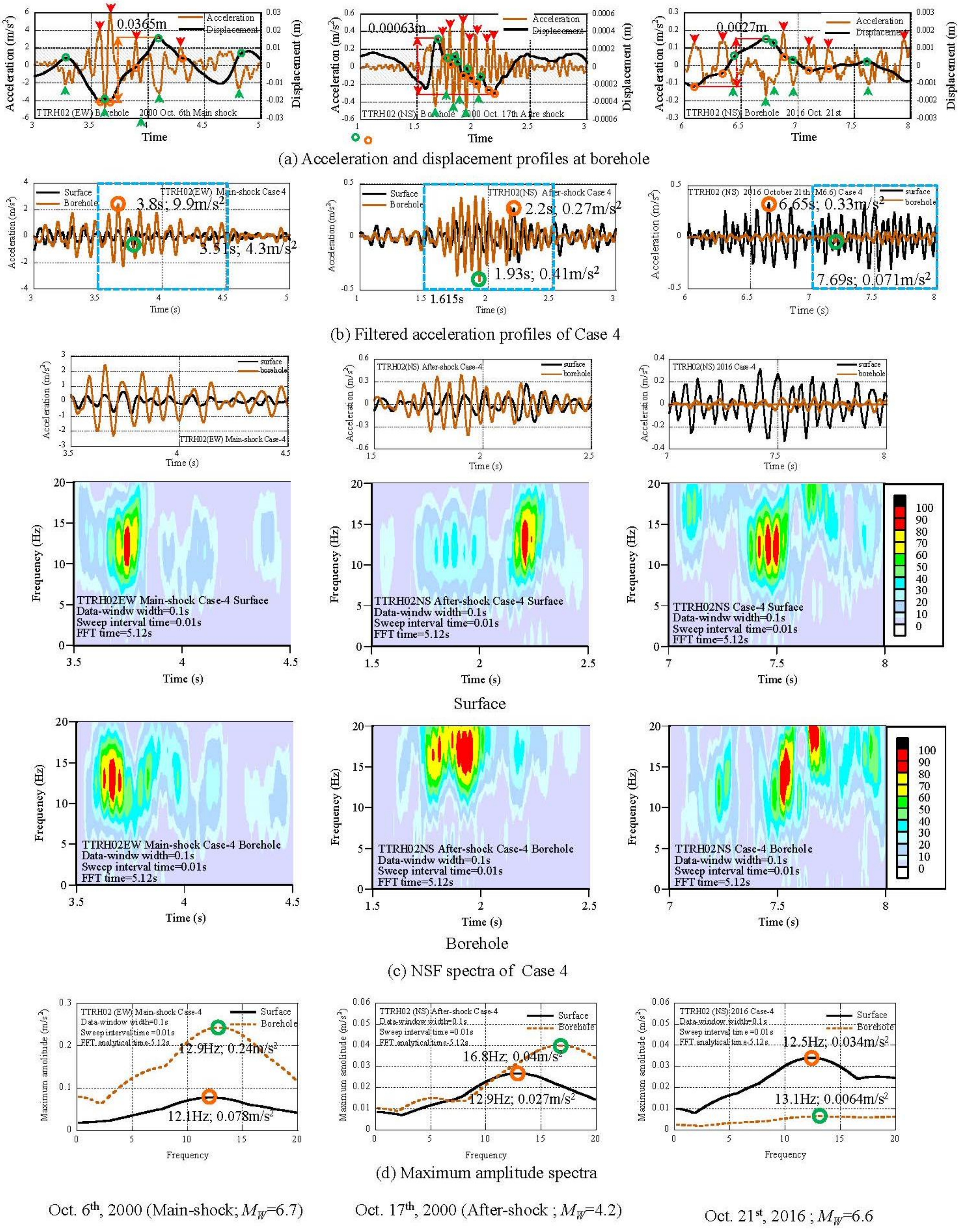


Fig. 8 Wave shape analysis of seismic records in three seismic events; TTRH02

the other hand the $P_{MA.B}$ scattered from $10^{-3}$m/s$^2$ to $10^{-1}$m/s$^2$.

• The $R_{S/B}$ were smaller than 1.0 in the main-shock and the aftershock in 2000 but the $R_{S/B}$ of the seismic records (2016) was 5.3, which apparently suggested an unnatural amplification at the borehole in the seismic records (2000).

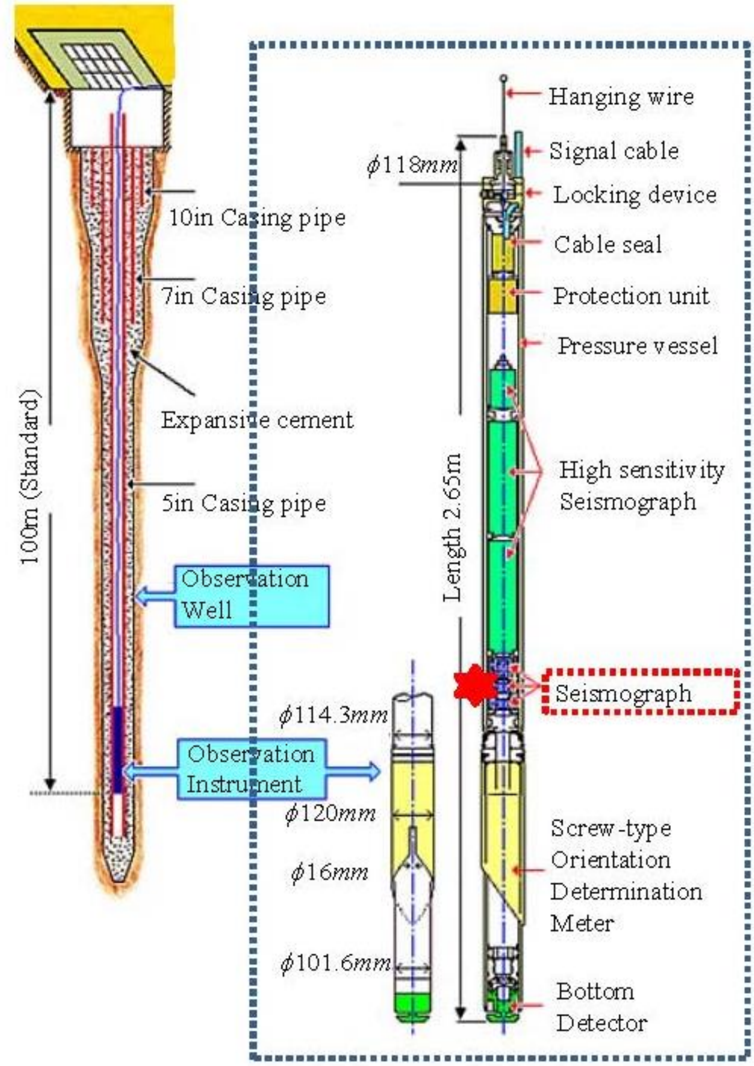


Fig. 9 Collision and Backlash of seismograph in casing pipe

Table 10 $P_A$, $R_P$ and $R_{S/B}$ in filtered acceleration profiles of IWTH25

| *case* | N-S | | | E-W | | | U-D | | |
|---|---|---|---|---|---|---|---|---|---|
| | $P_{A,S}$; $R_P$ | $P_{A,B}$; $R_P$ | $R_{S/B}$ | $P_{A,S}$; $R_P$ | $P_{A,B}$; $R_P$ | $R_{S/B}$ | $P_{A,S}$; $R_P$ | $P_{A,B}$; $R_P$ | $R_{S/B}$ |
| 0 | 11.4; 1.0 | 10.4; 1.0 | 1.10 | 14.3; 1.0 | 7.5; 1.0 | 1.92 | 39; 1.0 | 6.8; 1.0 | 5.68 |
| 1 | 3.5; 0.30 | 1.1; 0.11 | 3.17 | 3.2; 0.22 | 1.4; 0.18 | 2.32 | 1.98; 0.05 | 1.5; 0.22 | 1.32 |
| 2 | 3.5; 0.30 | 2.5; 0.24 | 2.22 | 6.5; 0.45 | 3.7; 0.49 | 1.74 | 7.4; 0.19 | 1.6; 0.24 | 4.53 |
| 3 | 3.5; 0.30 | 3.8; 0.37 | 1.85 | **7.9**; **0.55** | 3.5; 0.47 | 2.27 | 14.0; 0.36 | 3.6; **0.53** | 3.89 |
| 4 | 3.5; 0.30 | **6.8**; **0.65** | **0.97** | **7.7**; **0.54** | **6.5**; **0.87** | 1.18 | **27**; **0.69** | **5.6**; **0.83** | 4.71 |

The author surveyed the previous reports of NIED in order to make clear the occurrence mechanism of the unnatural amplification in the seismic records on 2000 and noticed the replacement of the seismograph from SMAX-MDK to KiK-net06 in 2008 (Kunugi *et al*. 2009). From the information of the replacement of seismograph the author got an occurrence mechanism by the mechanical amplification of the seismograph in the casing pipe. The measurement system at the borehole of KiK-net is illustrated in Fig. 9.

### *3.3 Seismic records of IWTH25*

The $P_{A,S}$ of 38.6 m/s$^2$ in IWTH25(U-D) during Iwate-Miyagi Nairiku earthquake in 2008 is the largest $P_{A,S}$ in the database of the K-NET and the KiK net. The occurrence mechanism was investigated by researchers. One was "Trampoline effect" by the amplification in the surface soil (Aoi *et al*. 2010). The others were the mechanical amplification in the measurement system: "rocking mode of observation house" (Ohmachi *et al*. 2011) and "induced pulse waves by the up-lift of observation house" (Kamagata

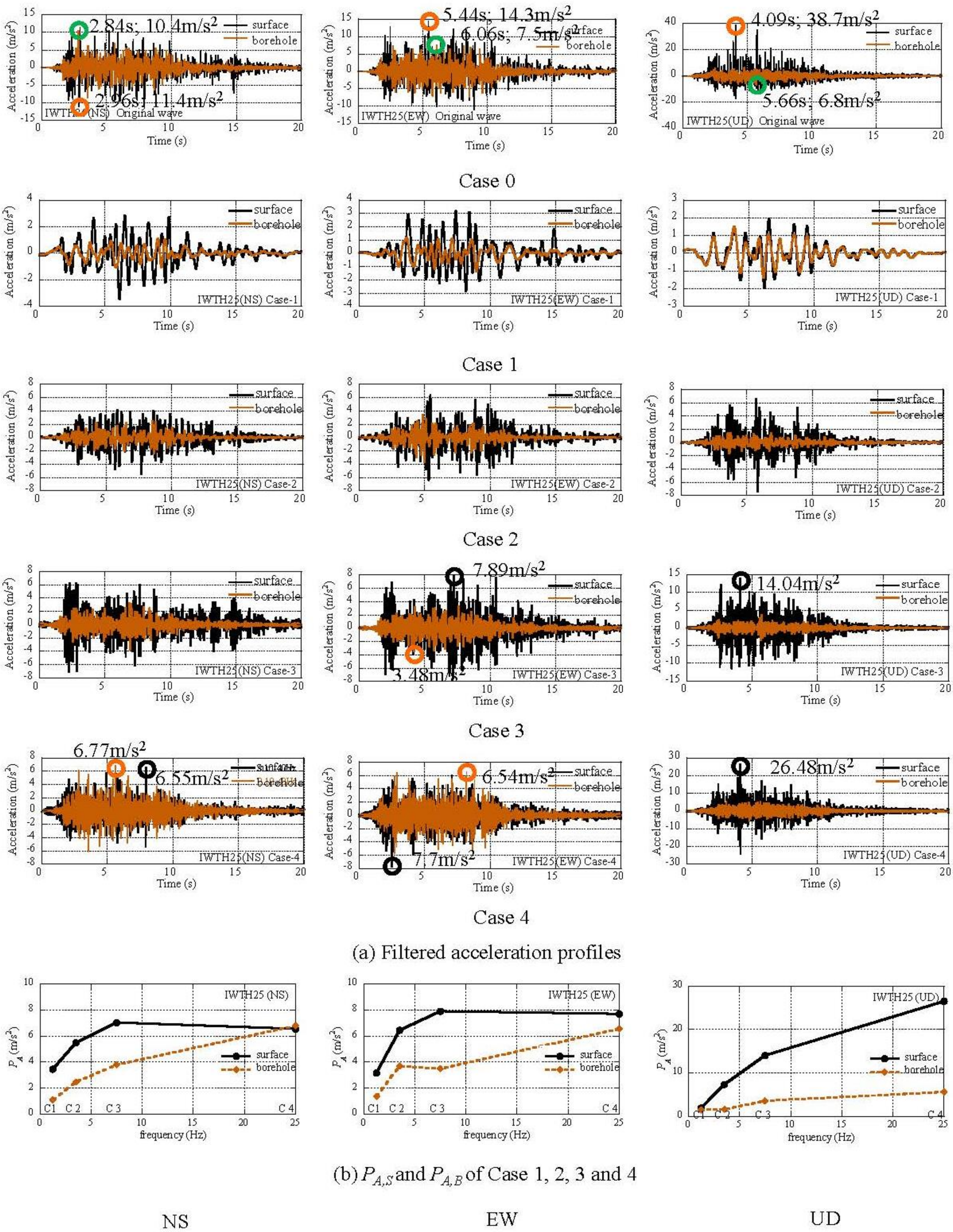


Fig. 10 Filtered acceleration profiles of IWTH25

and Takewaki 2017).

The author newly focused on the singular pulse waves at the borehole of IWTH25 and investigated them by the wave shape analysis. The filtered acceleration profiles of Case 0, 1, 2, 3 and 4 are illustrated as shown in Fig. 10(a). The $P_{A,S}$ and the $P_{A,B}$ of Case 1, 2, 3 and 4 are illustrated coupling

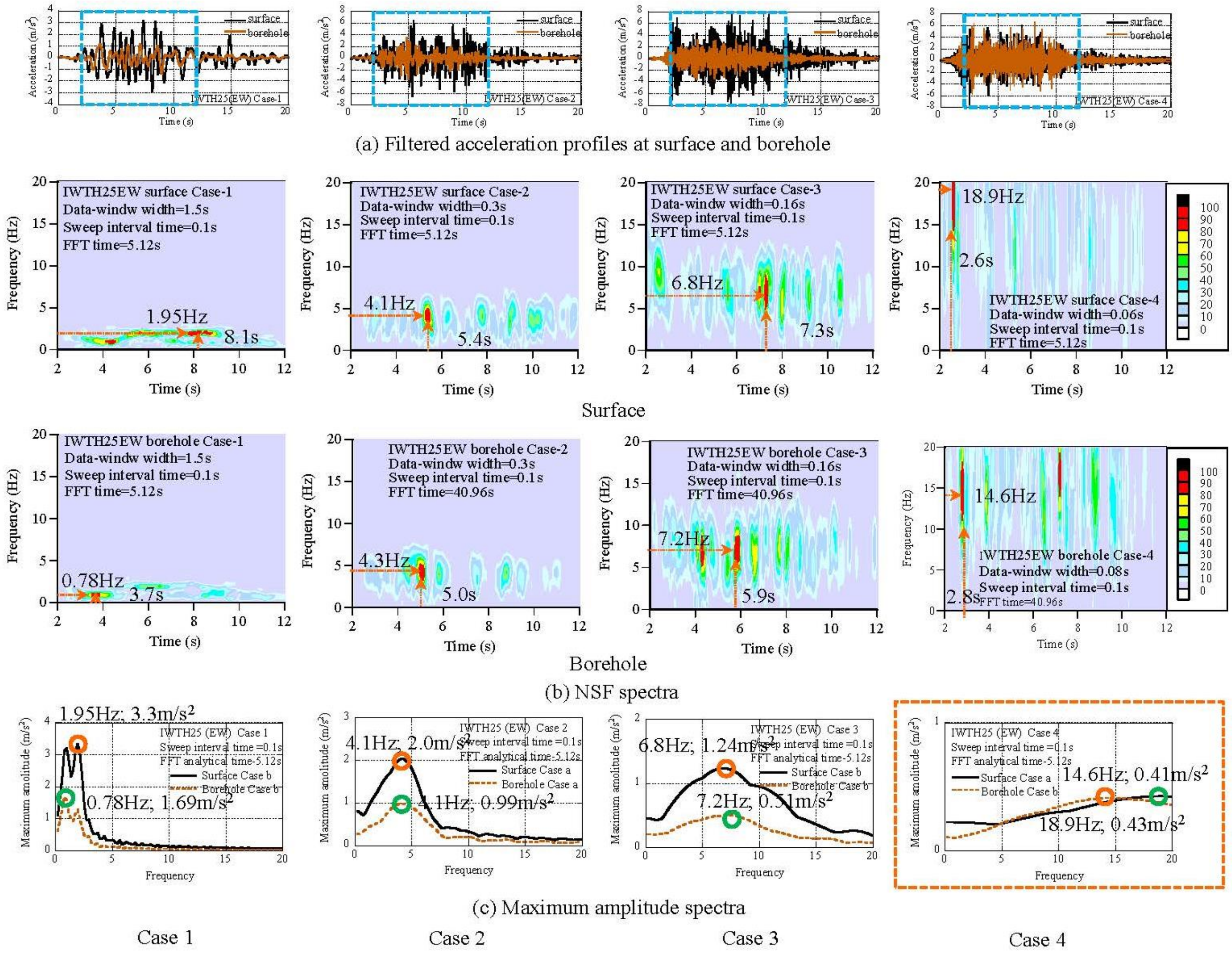


Fig. 11 NSF spectra of filtered acceleration profiles; IWTH25(E-W)

with the frequency $(f_{L2} + f_{L3})/2$ in Fig. 10(b). The $P_A$ at the surface and the borehole are listed with the $R_P$ ($P_A$ ratio of Case 1, 2, 3 and 4 by Case 0) and the $R_{S/B}$ in Table 10.

The property of the $P_{A,S}$, the $P_{A,B}$, the $R_P$ and the $R_{S/B}$ were evaluated as follows.

- In N-S component, the $P_{A,B}$ and the $R_P$ in Case 1 and 4 were 1.1 m/s$^2$, 6.8 m/s$^2$ and 0.11, 0.65 and the $R_{S/B}$ in Case 1 and 4 were 3.17 and 0.97. These values suggested that pulse waves at the borehole were mainly caused by the frequency components higher than 10Hz and the pulse waves at the borehole was caused by a local amplification at the borehole.
- In E-W component, the $P_{A,B}$, the $R_P$ and $R_{S/B}$ in Case 4 were 6.5 m/s$^2$, 0.87 and 1.18, which were close to those of 6.8 m/s$^2$, 0.65 and 0.97 in N-S component. These values suggested same occurrence mechanism in N-S and E-W components.
- In U-D component, the $P_{A,B}$, and the $R_P$ in Case 4 were 5.6 m/s$^2$ and 0.83 which were also close to of N-S and E-W component. On the other hands the $R_{S/B}$ of 4.71 differed from those of 0.97 and 1.18 in N-S and E-W components, which was estimated to be related to the singular pulse waves at the surface with the $P_{A,S}$ of 26.5 m/s$^2$.

Table 11 $P_{MA}$ at surface and borehole and $R_{S/B}$ of IWTH25

| Case | N-S | | | E-W | | | U-D | | |
|---|---|---|---|---|---|---|---|---|---|
| | $P_{MA,S}$ | $P_{MA,B}$ | $R_{S/B}$ | $P_{MA,S}$ | $P_{MA,B}$ | $R_{S/B}$ | $P_{MA,S}$ | $P_{MA,B}$ | $R_{S/B}$ |
| 1 | 2.9 | 1.12 | 2.59 | 3.3 | 1.69 | 1.93 | 1.93 | 1.67 | 1.16 |
| 2 | 1.87 | 0.65 | 2.88 | 2.0 | 0.99 | 2.02 | 2.0 | 0.44 | 4.55 |
| 3 | 1.01 | 0.54 | 1.87 | 1.24 | 0.51 | 2.43 | 1.89 | 0.59 | 3.20 |
| 4 | 0.42 | 0.38 | **1.11** | 0.43 | 0.41 | **1.05** | 1.57 | 0.27 | 5.81 |

The $R_{S/B}$ of 0.97 (N-S) and 1.18 (E-W) in Case 4 were the smallest in Case 1, 2, 3 and 4, which is similar to those of 0.51 (N-S) and 0.45 (E-W) in TTRH02 as shown in Table 5.

Further, the acceleration profiles at the surface and the borehole of Case 1, 2, 3 and 4 in IWTH25 (E-W) from 2 s to 12 s (enclosed by dotted rectangle in Fig. 11(a)) were analyzed by using the NSF spectra with three cases of $t_a$ and the suitable $t_a$ was selected by the condition of the minimum $t_a$>1/ $f_{MA}$. The NSF spectra with the suitable $t_a$ are illustrated as shown in Fig.11(b). The maximum amplitude spectra at the surface and the borehole are compared in Fig. 11(c). The $P_{MA,S}$, the $P_{MA,B}$, and the $R_{S/B}$ of Case 1, 2, 3 and 4 are listed in Table 11.

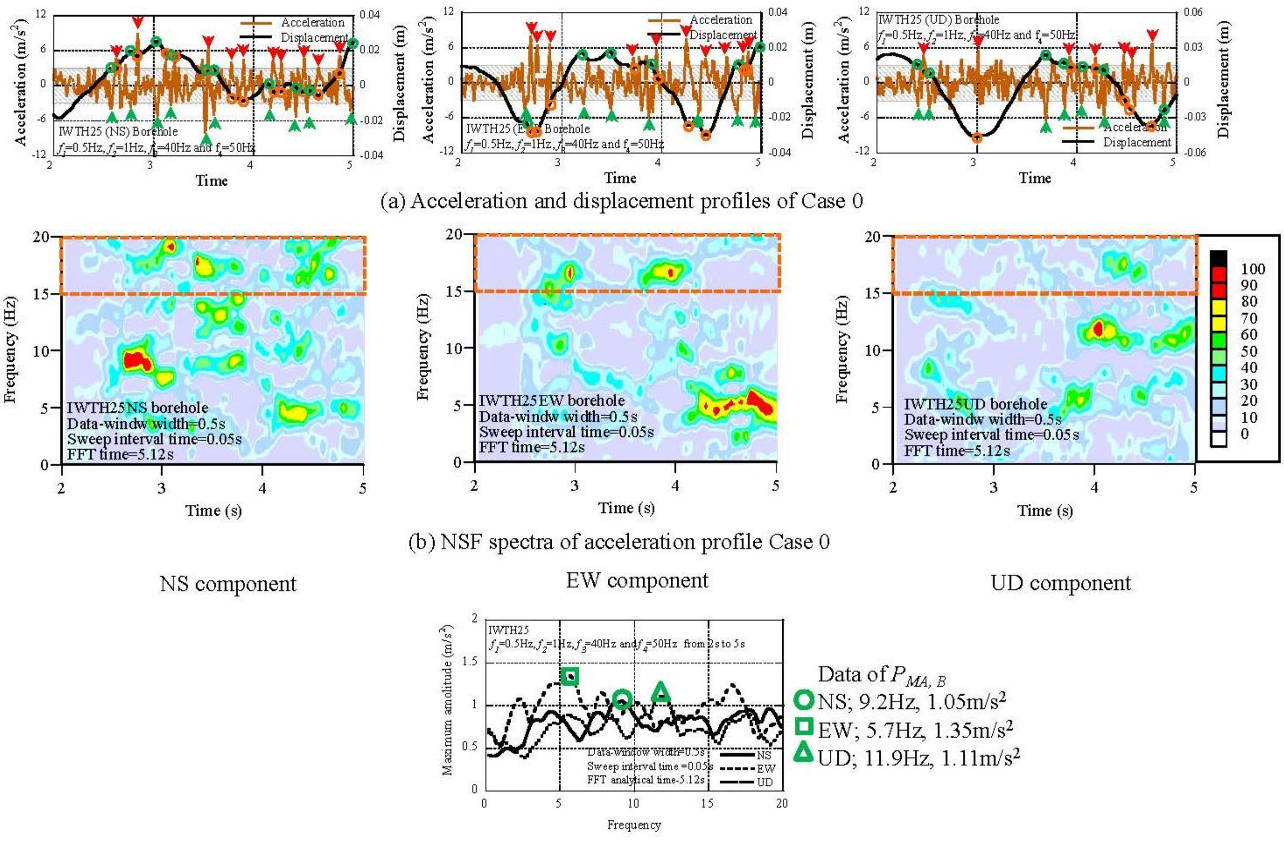

(a) Acceleration and displacement profiles of Case 0

(b) NSF spectra of acceleration profile Case 0

(c) Maximum amplitude spectra

Fig. 12 Wave shape analysis of seismic records; IWTH25

The properties of the dominant components in IWTH25 were derived as follows.

- In the filtered acceleration profiles of Case 1, 2 and 3 the profile at the surface exceeded those at the borehole, which was considered as the natural amplification in the surface soil.
- In the filtered acceleration profiles of Case 4 the profile at the borehole was close to that at the surface, which was considered as the singular amplification at the borehole.
- The $P_{MA,\,S}$ occurred after the $P_{MA,\,B}$ in Case 1, 2 and 3, which suggested that the dominant components were amplified in the propagation process from the borehole to the surface.
- The $P_{MA,\,B}$ in Case 4 occurred at 2.8s, which was later than the occurrence time of the $P_{MA,\,S}$ at 2.6s, which was unnatural amplification from the view point of wave propagation pass.
- The A.R. of 1.11 (N-S), 1.05 (E-W) in Case 4 were smaller than those in Case 1, 2 and 3, which were considered as an unnatural amplification at the borehole.

These analytical results indicated that the pulse waves at the boreholes in case 4 of IWTH25 were estimated to be caused by the similar amplification mechanism of pulse waves in TTRH02.

The filtered acceleration profiles of Case 0 at the borehole of IWTH25 from 2s to 5s are illustrated with the double integrated displacement profiles as shown in Fig. 12(a). Further, the acceleration profiles were analyzed by the NSF spectra with $t_a$ of 0.5 s and $\Delta T$ of 0.05 s, which are illustrated in Fig. 12(b). The maximum amplitude spectra of N-S, E-W and U-D components are illustrated in Fig. 12(c). The properties of pulse waves in IWTH25 were derived as follows.

- The positive pulses (red arrow) with the $P_{A,\,B}$ greater than 3 m/s$^2$ in the acceleration profile (brown line) corresponded to the downward reversal points (red circle) in the displacement profile and the negative pulses (green arrow) with the $P_{A,\,B}$ smaller than -3 m/s$^2$ corresponded to the upward reversal points (green circle) in the displacement profile as shown in Fig. 12(a).
- The dominant components were scattered in the frequency range from 15Hz to 20Hz (enclosed by dotted rectangle) as shown in Fig. 12(b), especially the pulse waves with $P_{A,B}$>3 m/s$^2$ were composed of the components of 15Hz or more.
- The maximum amplitude of N-S, E-W and U-D components were uniformly scattered from 0.5 m/s$^2$ to 1.5 m/s$^2$, which were considered as the radiated components at the seismic fault.

Based on the derived properties of the dominant components, the pulse waves at the borehole in case 4 of IWTH25 were estimated to be caused by the backlash of the seismograph itself in the casing pipe.

Table 12 $f_{MA,B}$(Hz), $P_{MA,B}$(m/s$^2$), $P_{MD,B}$(m), $f_{Ave}$, and $f_{S.D}$ of IWTH25 and TTRH02

| *case* | IWTH25 (E-W) | | | TTRH02 (E-W) | | | $f_{MA,B}$ | | |
|---|---|---|---|---|---|---|---|---|---|
| | $f_{MA,B}$ | $P_{MA,B}$ | $P_{MD,B}$ | $f_{MA,B}$ | $P_{MA,B}$ | $P_{MD,B}$ | $f_{Ave}$ | $f_{S.D}$ | R.D. |
| 1 | 0.78 | 1.69 | $7.0\times10^{-2}$ | 1.37 | 0.80 | $1.1\times10^{-2}$ | 1.08 | 0.42 | $3.9\times10^{-1}$ |
| 2 | 4.1 | 0.99 | $1.5\times10^{-3}$ | 3.3 | 0.52 | $1.2\times10^{-3}$ | 3.7 | 0.57 | $1.5\times10^{-1}$ |
| 3 | 7.2 | 0.51 | $2.5\times10^{-4}$ | 8.4 | 0.54 | $1.9\times10^{-4}$ | 7.8 | 0.85 | $1.1\times10^{-1}$ |
| 4 | 14.6 | 0.41 | $4.9\times10^{-5}$ | 13.9 | 0.156 | $2.0\times10^{-5}$ | 14.3 | 0.49 | **$3.0\times10^{-2}$** |

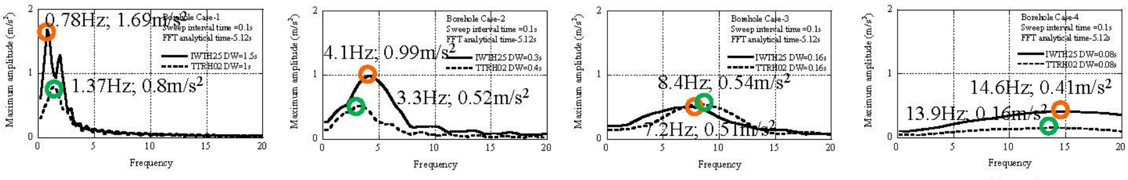


(a) Comparison of maximum amplitude spectra ; IWTH25 (EW) and TTRH02 (EW)

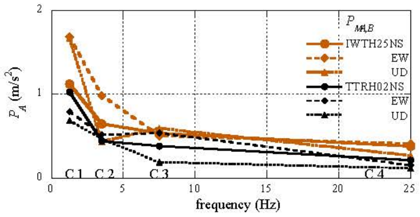


(b) $P_{A,B}$ of IWTH25 and TTRH02

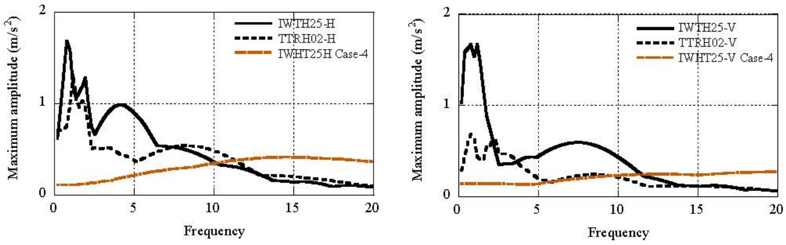


(c) Envelope maximum amplitude spectra; IWTH25 and TTRH02

Fig. 13 Maximum amplitude spectra of IWTH25 and TTRH02

### 3.4 *Maximum amplitude spectra of IWTH25 (E-W) and TTRH02 (E-W)*

The maximum displacement amplitude ($P_{MD}$) correspondent to the $P_{MA}$ was calculated by Eq. (4).

$$P_{MD} = P_{MA} / (2\pi f_{MA})^2 \tag{4}$$

The $f_{MA,B}$, the $P_{MA,B}$, and the $P_{MD,B}$ of IWTH25 (E-W) and TTRH02 (E-W) are listed in Table 12. In addition, the average ($f_{Ave.}$), the standard deviation ($f_{S.D.}$) and the relative deviation ($f_{S.D.}/f_{Ave}$; R.D.) of $f_{MA,B}$ in the seismic records of IWTH25 and TTRH02 were listed in Table 12.

The maximum amplitude spectra ($S_{MA}$ ($\omega_i$)) of IWTH25(E-W) and TTRH02(E-W) are compared in Fig. 13(a). The $P_{MA,B}$ in Case 1, 2, 3 and 4 of IWTH25 and TTRH02 are illustrated coupling with the frequency of ($f_{L2}+f_{L3}$)/2 in Fig. 13(b).

The singular pulse waves at the borehole were quantitatively evaluated as follows.

- The collision was estimated as one of the amplification factors in the displacement amplitude from $10^{-4}$m to $10^{-1}$m and in the frequency lower than 10Hz.
- The backlash was caused in the displacement amplitude from $10^{-5}$ m to $10^{-4}$ m and in the frequency higher than 10Hz.
- The R.D. with the order of $10^{-1}$ was detected in Case 1, 2 and 3, which were estimated to be caused by the fault activity and the propagation pass including the mechanical amplification (collision) by the seismograph.
- The R.D. of 0.03 in Case 4 suggested the same occurrence mechanism and the $f_{Ave}$ of 14.3Hz was related to the backlash of the seismograph.

In conclusion, the maximum amplitude spectrum of Case 4 in IWTH25 (brown dotted line in Fig. 13(c)) was eliminated from the envelope amplitude spectra of IWTH25. The maximum amplitude spectrum of the horizontal component was derived as the envelope of N-S and E-W components. The envelope of maximum amplitude spectra at the boreholes of TTRH02 and IWTH25 are illustrated in Fig. 13(c).

## 4. Conclusions

Most of the shear wave velocity values at the borehole of KiK-net are more than 700 m/s$^2$, which satisfy the condition of the engineering bedrock (700 m/s$^2$) for the NPPs in Japan. Therefore, the seismic records at the borehole are useful as the database for the seismic design. The author selected the database of KiK-net and analyzed them by the wave shape analysis. In the research the author detected the singular pulse waves in the seismic records at borehole of TTRH02 during the main-shock of Tottori-ken Seibu earthquake on 2000 ($M_W$:6.8).

The filtering procedure by the band-pass filter was newly introduced to improve the analytical accuracy of dominant components. The properties of the pulse waves were identified as follows.

• The singular pulse waves at the borehole in the seismic records were composed of components in the frequency higher than 10Hz.

• The amplitude values at the borehole were larger than those at the surface in the frequency from 5Hz to 40Hz.

Similar singular pulse waves were detected at the borehole of the after-shock on 2000 ($M_J$:4.2), while no singular pulse waves were detected at the borehole of the seismic record during the seismic event on 2016 ($M_W$:6.6). The author focused on the replacement of the seismograph from SMAC-MDK to KiK-net06 in 2008 and estimated the mechanical vibration of the seismograph in the casing pipe as the occurrence mechanism of the singular pulse waves.

The discriminated vibration state was estimated as two types of mechanical vibration by the seismograph in the casing pipe as follows.

• The collision between the seismograph and the casing pipe

• The backlash of seismograph itself

The vibration state of the singular pulse waves was investigated by the double integrated displacement profile and the synchrony of pulse waves in the acceleration profiles and the reversal points in the displacement profiles was detected. Further, the $P_{MD,B}$ was evaluated as follows.

• The $P_{MD,B}$ from $10^{-4}$m to $10^{-1}$m in the frequency lower than 10Hz was related to the fault activity and the propagation pass including the mechanical amplification (collision) by the seismograph in the casing pipe.

• The $P_{MD,B}$ from $10^{-5}$m to $10^{-4}$m in the frequency higher than 10Hz was mainly related to the backlash of seismograph itself in the casing pipe.

Furthermore, singular pulse waves were detected in the seismic records at the borehole of IWTH25 during the Iwate-Miyagi Nairiku earthquake on 2008. A similar relationship between the pulse waves in the acceleration profile and the reversal and inflection points in the displacement profile were detected. Further the similarity of pulse waves in IWTH25 and TTRH02 was detected in the relative deviation of frequency ($f_{MA,B}$) in Case 4 and the frequency of backlash was estimated 14Hz. Therefore, the pulse waves in Case 4 of IWTH25 were estimated to be caused by the backlash of the seismograph in the casing pipe similar to the pulse waves in TTRH02.

The seismic design waves are set on basis of various code (Ucar, T. and Merter, O. (2019)). The findings in this paper are applicable to select the database of seismic records for the seismic design. Moreover, the wave shape analysis can be used to identify the occurrence mechanism of pulse waves in the seismic record, such as the non-linear interaction between the building and side-soil (Kamagata and Takewaki (2013a)), which brought a new perspective for the research of the soil-structure interaction (Khazaei, J. (2017), Cai, Y., *et al*. (2018)).

## Acknowledgments

The author would like to thank NIED for providing seismic records of KiK-net and would like to thank Editage (www.editage.jp) for English language editing.

## References

. Kobayashi, G., Sugino, H., Tsutsumi, H., and Ebisawa, K. (2014), "Guidance for evaluation of seismic ground motion from diffuse seismicity", JNES-RE-Report Series, JNES-RE-2013-2045, Japan Nuclear Energy Safety Organization.

Aoi, S., Kunugi, T. and Fujiwara, H. (2010), "Trampoline effect in extreme ground motion", *Science,* **322**(5902), 727-730. 10.1126/science.1163113.

Cai, Y., Lee, V.W. and Trifunac, M.D. (2018), "In-plane soil-structure interaction excited by incident plane SV waves", *Soil Dyn. Earthq. Eng.*, **105**, 224-230. https://doi.org/10.1016/j.soildyn.2017.11.002.

Geospatial Information Authority of Japan (2008), "GPS stations detect crustal deformation caused by the Iwate-Miyagi Nairiku Earthquake in 2008", *Front. Built. Environ*., **3**(13), https://doi.org/10.3389/fbuil.2017.00013.

Horikawa, H., Sekiguchi, H., Iwata, T. and Sugiyama, Y. (2001). "A fault model of the 2000 Tottori-ken Seibu earthquake", Active fault and Palaeoseismicity Research Report, **1**, 27-40.

Iwata, T. (2002). Source model of the 2000 Tottori-ken Seibu earthquake and near-source strong ground motion. *In Proceedings of 11th Japan Earthq. Eng. Symp.*

Japan Nuclear Energy Safety Organization (2009), "Analysis of seismic records on non-linear interaction between the reactor building and surrounding soil", *JNES J-000-2010-00013* (in Japanese), http://warp.da.ndl.go.jp/info:ndljp/pid/10207746/www.nsr.go.jp/archive/jnes/atom-pdf/seika/000016346.pdf.

Kamagata, S. (2009), "Non-stationary Property of Niigata-ken Chuetsu-oki Earthquake on Kashiwazaki-Kariwa Nuclear Power Plants (Occurrence mechanism of Pulse-like wave), *Annual meeting of Architectural Institute of Japan, 2009* (in Japanese), https://www.aij.or.jp/jpn/pdf/2009taikai/data/pdf/B/21504.pdf.

Kamagata, S. and Takewaki, I. (2013a), "Occurrence mechanism of recent large earthquake ground motions at nuclear power plant sites in Japan under soil-structure interaction", *Earthq. Struct*., **4**(5), 557-585. https://doi.org/10.12989/eas.2013.4.5.557.

Kamagata, S. and Takewaki, I. (2013b), "New insights into seismic behavior of building and surrounding soil at Hamaoka nuclear power station during Suruga Bay earthquake in 2009", *Soil Dyn. Earthq. Eng.*, **53**, 73-91. https://doi.org/10.1016/j.soildyn.2013.06.007.

Kamagata, S. and Takewaki, I. (2015), "Analysis of ground motion amplification during soil liquefaction via nonstationary fourier spectra", *Int. J. Geomech*., **16**(5) C4015002, https://doi.org/10.1061/(ASCE)GM.1943-5622.0000549.

Kamagata, S. and Takewaki, I. (2017), "Occurrence mechanism of large acceleration in KiK-net seismic records during Iwate-Miyagi Nairiku earthquake in 2008", *Front. Built Environ*., **3**(13), https://doi.org/10.3389/fbuil.2017.00013.

Kamagata, S. and Takewaki, I. (2018), "Various occurrence mechanisms of large acceleration over 20m/s$^2$ and its suitability in design use", *Front. Built Environ*., **4**(3), https://doi.org/10.3389/fbuil.2018.00003.

Khazaei, J., Amiri, A. and Khalilpour, M., (2017), "Seismic evaluation of soil-foundation-structure interaction: Direct and Cone model", *Earthq. Struct*., **12**(2), 251-262. https://doi.org/10.12989/eas.2017.12.2.000.

Kojima, K., Kamagata, S. and Takewaki, I. (2014), "A new interpretation of large amplitude earthquake acceleration from non-linear local soil-structure interaction", *Nucl. Eng. Des.*, **273**, 271-287. https://doi.org/10.1016/j.nucengdes.2014.03.023.

Kunugi, T. Aoi, S. Fujiwara, H. and Nakamura, H. (2009), "Strong-motion Seismograph Networks (K-NET, KiK-net) of National Research Institute for Earth Science and Disaster Resilience", Natural Disaster Research Council. http://www.dpri.kyoto-u.ac.jp/ndic/sympo/s46/10kunugi.pdf.

National Institute of Advanced Industrial Science and Technology (2018), "Research Institute of Earthquake and Volcano Geology", https://unit.aist.go.jp/ievg/en/index.html.

National Research Institute for Earth Science and Disaster Prevention (2018), "Strong-motion Seismograph Networks (K-NET, KiK-net)", http://www.kyoshin.bosai.go.jp.

National Research Institute for Earth Science and Disaster Prevention (2008), "Iwate-Miyagi Nairiku earthquake in 2008: Fault model based on permanent displacement by KiK-net and the GPS displacement data of Technical Report of the Geospatial Information Authority of Japan", https://www.jishin.go.jp/main/chousa/08jun_iwate_miyagi2/p07.htm.

Nuclear Regulation Authority (2013a), "Outline of New Regulatory Requirements (Design Basis)", https://www.nsr.go.jp/data/000067117.pdf.

Nuclear Regulation Authority (2013b), "Outline of New Regulatory Requirements for Light Water Nuclear Power Plants (Earthquakes and Tsunamis), https://www.nsr.go.jp/data/000067118.pdf, on Mar. 2018.

Ohmachi, T., INOUE, S., Mizuno K. and Yamada, M. (2011), "Estimated cause of extreme acceleration records at the KiK-net IWTH25 station during the 2008 Iwate-Miyagi Nairiku earthquake, Japan", *T. Jpn. Assoc. Earthq. Eng.*, **11**(1), 32-47

Papagiannopoulos, G.A., Hatzigeorgiou, G.D. and Beskos, D.E. (2013), "Recovery of spectral absolute acceleration and spectral relative velocity from their pseudo-spectral counterparts", *Earthq. Struct.*, **4**(5), 489-508

Rahgozar, N., Moghadam, A.S. and Aziminejad, A, (2017), "Response of self-centering braced frame to near-field pulse-like ground motion", *Struct. Eng. Mech.*, **62**(4). https://doi.org/10.12989/sem.2017.62.4.000.

Ricker, N. (1942), "Further developments in the wavelet theory of seismogram structure", *Bull. Seismol. Soc. Am.*, **33**(3), 197-228.

Strasser, F. and Bommer, J.J. (2009), "Large-amplitude ground motion recordings and their interpretations", *Soil Dyn. Earthq. Eng.*, **29**(10), 1305-1329. https://doi.org/10.1016/j.soildyn.2009.04.001.

Tajammolian, H., Khoshnoudian, F. and Bokaeian, V. (2016) "Seismic responses of asymmetric steel structures isolated with the TCFP subjected to mathematical near-fault pulse methods", *Smart Struct. Syst*., **18**(5), 931-953. http://dx.doi.org/10.12989/sss.2016.18.5.931.

Trifunac, M.D. (1971), "Response envelope spectrum and interpretation of strong earthquake ground motion", *Bull. Seismol. Soc. Am*., **61**(2), 343-356.

Ucar, T. and Merter, O. (2019), "Effects of design spectral shape on inelastic response of RC frames subjected to spectrum matched ground motion", *Struct. Eng. Mech.*, **69**(3), https://doi.org/10.12989/sem.2019.69.3.293.

Zhai, C.H., Zheng, Z, Li, S., Pan, X. and Xie, L.L. (2016), "Seismic response of nonstructural components considering the near-fault pulse-like ground motions", *Earthq. Struct.*, **10**(5), 1213-1232.

*CC*